NeuroImage 317 (2025) 121272

Contents lists available at ScienceDirect

NeuroImage

journal homepage: www.elsevier.com/locate/ynimg

Age- and sex-specific normative curves for intracranial and ventricular volumes from head CT scans

Pedro Vinicius Alves Silva [a,*], Bruna Garbes Goncalves Pinto [a], Gabriel Ferracioli [a], Klaus Schumacher [a], Artur Jose Marques Paulo [a], Luis Alvaro Correia [a], Mariana Curi [b], Mateus Trinconi Cunha [a,c], Joselisa Peres Queiroz de Paiva [a], Tatiana Larissa Medeiros Arcanjo Marques [a], Rafael Maffei Loureiro [a]

[a] Hospital Israelita Albert Einstein, Imaging Department, São Paulo, 05652-000, São Paulo, Brazil
[b] Institute of Mathematical and Computer Sciences, Universidade de São Paulo, São Carlos, 13566590, São Paulo, Brazil
[c] Thoracic and Head and Neck Medical Oncology, The University of Texas M.D. Anderson Cancer Center, Houston, 77030, TX, USA

ARTICLE INFO

Keywords:
Brain
Intracranial volume
Lateral ventricular volume
Computed tomography
GAMLSS
Growth curves
Normative data

ABSTRACT

This study aims to establish age- and sex-specific normative curves for intracranial (ICV) and lateral ventricular volumes (LVV) using computed tomography (CT), addressing a significant gap in the literature. A total of 2153 head CT scans were analyzed, using the Generalized Additive Model for Location, Scale, and Shape (GAMLSS) to model the nonlinear relationship between age and volume of the brain structures, independently by sex. Model quality was evaluated through chi-square adherence test and residual analysis. Bootstrap resampling was used to generate 95% confidence intervals for the centile estimates. The results reveal distinct growth patterns for ICV, which peaks early in life, and LVV, which increases throughout life. Significant sexual dimorphism was found, with males showing larger volumes for both structures. Brain charts detailing the mean and median trends and coefficient of variation are presented and compared with previously published normative ranges. These normative curves have the potential to serve as important tools for research and clinical practice, facilitating the differentiation between normal and pathological brain changes, particularly in settings where CT is more accessible than magnetic resonance imaging (MRI).

1. Introduction

Understanding brain volume and structure is essential for neuroimaging research and diagnosing brain disorders. Two key measurements in this context are intracranial volume (ICV) and lateral ventricular volume (LVV), both frequently measured by imaging techniques such as computed tomography (CT) and magnetic resonance imaging (MRI) (Breakey et al., 2017; Huff et al., 2019; Ritvanen et al., 2013; González-Villà et al., 2016). The ICV represents the total space within the skull, including the brain (encephalon), protective meninges, and cerebrospinal fluid. The value of ICV and its temporal variations have been identified as essential covariates in studies of neurodegenerative disorders, aging, and cognitive decline (van Loenhoud et al., 2018; Fang et al., 2022; Westman et al., 2013). Additionally, ICV is commonly used as a proxy for "brain reserve", reflecting the brain's capacity to withstand damage (Van Loenhoud et al., 2018). ICV is also valuable for diagnosing and monitoring conditions that affect cranial volume, such as microcephaly and craniosynostosis, and for evaluating brain growth in children. Moreover, it plays a crucial role in postoperative assessments of craniofacial surgeries and is applied in anthropological and forensic studies (Maragkos et al., 2021; Kalucki et al., 2020).

The lateral ventricular volume (LVV) refers to the combined volume of the lateral ventricles. While total cerebrospinal fluid volume reflects heterogeneous compartments (e.g., subarachnoid spaces, cisterns), LVV provides a direct marker of structural changes in conditions like hydrocephalus and neurodegenerative diseases, indicating brain atrophy or cerebrospinal fluid accumulation (Nestor et al., 2008; Kuller et al., 2005; Vita et al., 2006; Mosley et al., 2005). Moreover, in hydrocephalus, disproportionate LVV enlargement correlates with parenchymal compression and clinical dysfunction, making it a critical diagnostic criterion (Quon et al., 2021). By prioritizing LVV, normative curves align with radiological practice, enabling targeted assessment of pathologies where ventricular dynamics are central to diagnosis and monitoring (Hedderich et al., 2020; Pahwa et al., 2021). Beyond its clinical significance and integration into radiological practice, LVV

* Corresponding author.
E-mail address: alvespedros@outlook.com (P.V.A. Silva).

https://doi.org/10.1016/j.neuroimage.2025.121272
Received 1 November 2024; Received in revised form 2 May 2025; Accepted 14 May 2025
Available online 27 June 2025

segmentation is also less susceptible to partial volume effects than cerebrospinal fluid segmentation, enhancing its reliability for volumetric assessments (Tohka, 2014).

Manual measurement of ICV and LVV is labor-intensive and challenging to scale for large datasets (Huo et al., 2017; Klasson et al., 2015; Whitwell et al., 2001). However, advancements in imaging technology and computational power have facilitated the development of automated methods – primarily focused on MRI – significantly improving the efficiency and accessibility of volume estimation, including image-quality agnostic models like SynthSeg (Billot et al., 2023; Huisman et al., 2024; Malone et al., 2015; Sargolzaei et al., 2015).

Normative volumes for various brain structures have been estimated by combining datasets from studies of healthy controls (Peterson et al., 2018). However, specific normative curves for ICV and LVV derived from CT data are limited (Kellogg et al., 2023; Maragkos et al., 2021). Developing normative curves applicable to pediatric and adult populations is crucial to address this gap. Such curves would facilitate the accurate early diagnosis of pathological processes and the monitoring of therapeutic responses across a range of clinical settings (Cutler et al., 2020; Schipper et al., 2021). Several statistical models have been employed in the creation of these curves, including the Lambda-Mu-Sigma (LMS) method (T.J. Cole, 1992), fractional polynomial parametric smoothing (Bethlehem et al., 2022), and cubic penalized B-splines (Nasser et al., 2024), all of which served as references in our modeling process.

In low- and middle-income countries, relying on MRI for assessing intracranial volumes can be challenging due to limited resources (Geethanath and Vaughan, 2019; WHO, 2022). In these settings, CT scans offer a more affordable and accessible alternative. To address this need, our team developed the DeepCTE3D model for automatic segmentation and quantification of LVV and ICV from head CT scans (Moraes et al., 2023). However, the lack of comprehensive normative data has limited the model's broader utility. This study aims to establish age- and sex-specific normative curves for LVV and ICV using head CT scans, creating a foundation for effectively applying automated segmentation and quantification models in clinical practice.

2. Methods

2.1. Sample size

The sample size was determined using the methodology outlined by Bridges and Holler (Bridges and Holler, 2007) in their work on optimal sample size for pediatric neuropsychological normative studies. We assumed that the normal neuropsychological functioning observed in these studies reflects the typical functionality of a healthy central nervous system, which is often associated with normal intracranial and ventricular volumes. This approach was necessary given the lack of specific research addressing sample size for growth charts in CT brain volumetry. Based on their recommendations, we calculated that 50 individuals per age group and sex would be needed to achieve a confidence interval with a width of 0.28 z-score, resulting in a total of 1,900 scans. The distribution of these scans was stratified according to demographic data from the Brazilian Institute of Geography and Statistics (IBGE) (IBGE, 2024) (see Supplementary Table 1) and divided into 19 age groups, each spanning 5 years (0–4, 5–9, 10–14, 15–19...).

2.2. Data

Non-contrast head CT scans conducted at Hospital Israelita Albert Einstein, a large tertiary care center in Brazil, were included in this study. These scans were performed using different CT scanners. The selection process involved a retrospective search in the institutional Picture Archiving and Communication System (PACS) for reports containing the phrase 'encephalic parenchyma within normal limits.' Hence, we defined exams as normal based only on radiologic assessments. Scans lacking thin-section image series (i.e., pixel spacing greater than 1.3 mm), those with significant imaging artifacts, or missing metadata on age or sex were excluded. Scans whose reports indicated normal findings were automatically retrieved for inclusion. Exams were deidentified using the Radiological Society of North America Clinical Trial Processor, with customized scripts to retain relevant DICOM (Digital Imaging and Communications in Medicine) tags for serial identification, patient age, and sex.

2.3. Annotation pipeline

Volumetric data for intracranial and ventricular structures were acquired through manual segmentation of CT scans by ten researchers with health science backgrounds. Using a web-based version of 3D Slicer, they created binary masks independently validated by five board-certified neuroradiologists, each with over six years of experience. Considering that annotation and validation were conducted independently for each structure and the process was completed once the necessary sample size was reached, some exams were validated for ICV but not for LVV, and vice versa. Anatomical variants of the ventricles, such as the cavum septi pellucidi and cavum vergae, were excluded from LVV measurements due to their lack of direct communication with the ventricular system; however, these cases were retained in the study. ICV calculations inherently encompass all intracranial structures. A detailed description of the segmentation and validation process can be found in our previous work (Pinto et al., 2024).

2.4. Outliers

Within each age group, the distribution of LVV was analyzed to detect outliers using the interquartile range (IQR) method. In each age group, values outside the range of (25% centile - 1.5 IQR; 75% centile + 1.5 IQR) were considered outliers. This method ensures that the outlier selection is balanced across the entire distribution curve (Supplementary Figs. 1–4). To further evaluate these cases, all were subjected to qualitative inspection by two neuroradiologists to confirm that the scans did not have significant pathological abnormalities.

Ethical approval for this study was granted by the institutional ethics committee (CAAE: 52257521.8.0000.0071). The requirement for informed consent was waived due to the retrospective design of the study and the use of anonymized data.

2.5. Statistical analysis

Continuous variables are presented as medians and IQRs ($Q_{25\%}$ – $Q_{75\%}$) depending on their distribution. Normality was assessed using the Anderson–Darling test at a 5% significance level and a visual inspection of quantile–quantile (Q–Q) plots. Categorical variables are reported as frequencies and percentages. We employed a two-tailed Kruskal–Wallis test at a 5% significance level to evaluate the impact of image characteristics on volumetric measurements. The null hypothesis stated that there would be no difference between patient sexes in the median of ICV and LVV. The effect size was calculated using the η^2 statistic (Tomczak M., 2014), in which small, moderate, and large effects were defined as 0.01–0.06, 0.06–0.14, and ≥ 0.14, respectively (Cohen, 1988).

The 95% confidence intervals for the normative curves were generated using nonparametric bootstrapping (Stasinopoulos et al., 2022) with 1000 samples drawn with replacement.

2.6. Statistical modeling

We employed the Generalized Additive Models for Location, Shape, and Scale (GAMLSS) (Stasinopoulos et al., 2017), a flexible and adaptable framework recommended by the World Health Organization (Borghi et al., 2005) for modeling non-linear growth trajectories. This approach provides a mathematical framework to describe the relationship between the studied volumes and age, enhancing the interpretability of the results.

GAMLSS extends Generalized Linear Models (GLM), which are limited to modeling probability distributions from the exponential family (e.g., Normal, Bernoulli) and characteristics such as the mean in linear regression or the log of odds in logistic regression. GAMLSS broadens this approach by allowing the response variable to follow any probability distribution and enabling the modeling of up to four statistical moments, symbolized by the parameters μ, σ, ν, and τ, which, depending on the selected distribution, represent the mean, variance, skewness, and kurtosis, respectively.

The nonlinear relationship between age and the volume of the studied structures was modeled using fractional polynomials (Royston and Altman, 1994). This family of parametric smoothers has the functional form of $a+\beta_1 x_1^{p_1}+\beta_2 x_2^{p_2}+\cdots+\beta_n x_n^{p_n}$. The possible values of p_i parameters are (−2,-1,−0.5,0,0.5,1,2,3) and are selected along with the estimation of β coefficients by the GAMLSS package for up to n = 3. Because of this method's stricter nature compared to non-parametric smoother, it produced more parsimonious and clinically interpretable curves, minimizing spurious fluctuations in volume. The final models were selected as described in Section 2.7 and their mathematical description is presented below. The interpretation of its parameters, especially μ and σ, is a direct consequence of the choice of the distributions.

$$\begin{aligned} Y_{ICV} &\sim \text{Gamma}(\mu,\sigma) \\ \log(\mu) &= \alpha_\mu + \beta_{\mu,0} + \beta_{\mu,1}(age)^{p_{\mu,1}} + \beta_{\mu,2}(age)^{p_{\mu,2}} \\ \log(\sigma) &= \alpha_\sigma + \beta_{\sigma,0} + \beta_{\sigma,1}(age)^{p_{\sigma,1}} \end{aligned} \quad (1)$$

Where Y_{ICV} represents the intracranial volume in cm^3, β are the coefficients of fractional polynomials, and α is the model intercept. For the Gamma distribution, μ represents the mean, while σ is the coefficient of variation (CoV) - ratio between the standard deviation and the mean. In our context, this indicates that the mean volume increases faster than the standard deviation, meaning that variability becomes less significant relative to the absolute volume. For example, consider a male sample of 1-year-old children with a mean ICV of 1200 cm^3 and a standard deviation of 120 cm^3. The CoV, defined as the ratio of the standard deviation to the mean, is 0.1. Now consider a male sample of 75-year-old adults with a mean ICV of 1500 cm^3 and the same standard deviation of 120 cm^3; in this case, the CoV is 0.08. This reduction in CoV indicates that the relative variability among individuals in ICV decreases with age.

$$\begin{aligned} Y_{LVV} &\sim \text{BCT}(\mu,\sigma,\nu,\tau) \\ \log(\mu) &= \alpha_\mu + \beta_{\mu,0} + \beta_{\mu,1}(age)^{p_{\mu,1}} + \beta_{\mu,2}(age)^{p_{\mu,2}} \\ \log(\sigma) &= \alpha_\sigma + \beta_\sigma \text{age} \\ \nu &= \alpha_\nu \\ log(\tau) &= \alpha_\tau \end{aligned} \quad (2)$$

Y_{LVV} represents the lateral ventricular volume in cm^3, and for the Box–Cox-t (BCT) distribution, μ represents the median, $\sigma(\frac{\tau}{\tau-2})^{0.5}$ is approximately the coefficient of variation, ν controls the skewness, and τ controls the kurtosis. Models were independently fitted for each sex and subsequently used to calculate centile values.

Eqs. (1) and (2) were used to interpret the relationship between age and volume (Figs. 4 and 5). The centile curves were derived from these equations. Once the parameters ((μ,σ) for ICV and (μ,σ,ν,τ)) are determined for all ages, the distribution is fully defined, allowing the centiles to be calculated accordingly (Figs. 2 and 3).

2.7. Model selection and goodness of fit

Different probability distributions, selected based on the Akaike Information Criterion, were tested for the Lambda-Mu-Sigma (LMS), penalized B-splines, and fractional polynomials methods. The adequacy of the models was evaluated by inspecting three types of residuals. Randomized quantile residuals, which usually produce distributed residuals aside from sampling variability, were used to verify general deviations from the fitted distribution (Dunn and Smyth, 1996).

Q-statistics were used to evaluate the normality of residuals, aiding in the detection of inadequacies in the μ,σ,ν, and τ model parameters (Royston and Wright, 2000). Plots of the residuals and a thorough explanation are presented in the Supplementary Material Section 3.1.

Two board-certified neuroradiologists were actively involved in the fitting process to ensure the clinical relevance and interpretability of the curve trends. Their expertise was critical in validating that the generated curves accurately reflected expected anatomical variations and did not introduce clinically implausible patterns.

The goodness of fit of the final models was assessed using the chi-square adherence test at 5% significance level. The deviation of each volume from the model's mean was quantified in terms of standard deviations, referred to as the z-score. We calculated the percentiles for the z-scores and binned them in 25 intervals. Under the null hypothesis, the binned z-score data were expected to be uniformly distributed across percentile intervals. If the models accurately represent the volumetric distributions, each percentile interval should contain an equal number of exams.

2.8. Comparison of curves

The intracranial curves were compared with those of Satanin et al. (2024a) for children. To allow the comparison, we binned their non-integer age centiles as follows: individuals aged from 0 months to 5 months were considered as 0 years, from 6 months to 1.25 years as 1 year, from 1.5 to 2.25 as 2 years, and so on. Our lateral ventricular curves were compared with those from Maragkos et al. (2021) by grouping our age predictions into their respective bins and extracting the median of our quantiles. A Kruskal–Wallis test at a 5% significance level was then used to assess differences. The null hypothesis stated that both curves came from the same population.

2.9. Preliminary validation

A preliminary validation of the curve's potential to detect cases with a clinical condition was conducted with six cases. Their volumes were compared with the normative ranges by the z-scores of their volumes. The abnormality is detected if |z-score| > 2, which is equivalent to their location falling below the 2.5% curve or above the 97.5% curve.

3. Results

3.1. Data

A total of 2,166 exams were retrieved from the PACS. After excluding scans with missing metadata, 2,153 head CT scans met the inclusion criteria and were used in the study. The age range was 0–92 years for males and 0–95 years for females. The overall median age of the patients was 36 (18–52), with an overall range of 0–95 years. Of the participants, 1,061 (49.28%) were male, and 1,092 (50.72%) were female. Considering the intracranial and ventricle samples, no statistical difference was found in the ages of both.

Among the 1,092 male patients, 39 exams lacked specialist validation for ICV and 51 for LVV. Similarly, among the 1,092 female patients, 46 exams were not validated for ICV, and 70 were not validated for LVV. Volumes from non-validated exams were discarded from the fitting procedure for the respective structure (Fig. 1). No image

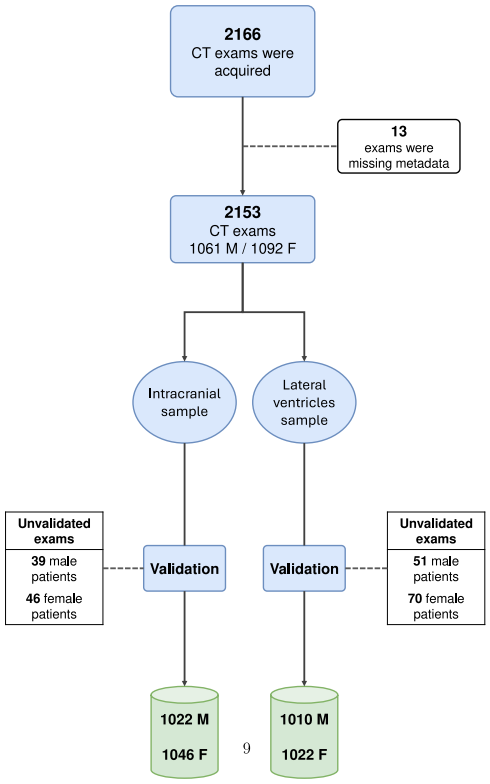

Fig. 1. Validation flow of CT exams. Segmentation masks not validated by specialists were removed from the fitting procedure.

Table 1
Age distribution of male and female patients between structures.

Age group	Intracranial Male	Intracranial Female	Ventricle Male	Ventricle Female
0–4	72	73	68	67
5–9	68	61	68	61
10–14	70	65	68	65
15–19	73	66	71	65
20–24	79	77	79	79
25–29	81	75	84	74
30–34	76	76	76	77
35–39	77	76	77	77
40–44	74	77	71	71
45–49	78	80	75	72
50–54	68	71	63	71
55–59	55	58	55	55
60–64	44	51	47	51
65–69	43	53	43	52
70–74	30	35	30	35
75–79	15	22	15	20
80–84	11	16	11	16
85–89	5	9	6	9
90+	3	5	3	5
Total	**1022**	**1046**	**1010**	**1022**

lacked validation for both the intracranial and the ventricular volume, and while they differ in number, 96% of patients are shared between the samples. The final distribution of each structure by sex is presented in Table 1.

The ICV masks resulted in a median volume of 1,349.98 (1255.93–1456.76) cm^3, while the median LVV was 12.81 (8.65–18.89) cm^3. When stratified by sex, females were observed to have smaller intracranial and ventricular volumes compared to males. No statistically significant difference was found between the median ages of both sexes. P-values and effect sizes are provided in Table 2.

3.2. Outliers

Of the 96 scans flagged as outliers based on the IQR, 87 showed age-appropriate brain parenchyma. Five had suboptimal segmentation. One scan revealed a cavum vergae, an anatomical variant. Two demonstrated signs of suspected normal pressure hydrocephalus (Supplementary Figures 5, 6, and 7), with one showing focal white matter hypoattenuation. Another scan showed the lateral ventricular roof enlargement, likely representing ischemic injury sequelae (Supplementary Figure 8).

3.3. Curves

Figs. 2 and 3 present the normative curves for intracranial and lateral ventricular volumes. The majority of the data points fall within these boundaries, and the chi-square test yielded a *p*-value of 1 for all fitted models, as expected if the centile curves accurately reproduce the data centiles (i.e., the number of observations between the 25%–50% and 50%–75% intervals is statistically the same). The curves also appear to accurately capture the non-linear trend between volume and age of the studied structures.

For the ICV models, a residual analysis (Supplementary Figures 11 to 14) indicates a slight overestimation of the mean ICV for male patients aged 29–34 years. Overall, there are no strong indications of misfit in the chosen distributions. Fig. 4 illustrates the trends in the mean and coefficient of variation (CoV) in the proposed models for ICV. The early rapid development (0–12.5 years) is effectively captured by the rapid increase in the mean of ICV and the decrease of CoV. While the CoV model consistently demonstrates a decline throughout adulthood for both sexes, visual assessment of the ICV model strongly suggests a more pronounced reduction in females compared to males. Future statistical analyses are expected to robustly confirm and further elucidate this apparent sex-specific trend. The wider confidence intervals of the centile estimates in the bootstrap analysis (Supplementary Figure 15) suggest that additional data is needed to accurately estimate key developmental milestones, such as the mean peak of ICV value and the growth rate throughout life.

For the male LVV curves, residual analysis (Supplementary Figures 16–19) indicated a possible underestimation of the median in individuals aged 8–14 years and the CoV in those aged 48–55 years. Additionally, there were signs of overestimation in the median for ages 15–21 years and in kurtosis for ages 22–28 years. For the female curves, we observed a potential overestimation of the median in individuals aged 44–50 years, while the median for ages 58–67 years and the kurtosis for ages 24–29 years appeared to be underestimated. Despite these indications, randomized quantile plots revealed no signs of overall model misspecification or misfit.

As shown in Fig. 5, lateral ventricular volumes tend to increase exponentially throughout life. In both males and females, the CoVs exhibited an approximately linear decrease, suggesting that ventricular volume is highly variable among infants but becomes more consistent among older individuals. Similar to the ICV curves, bootstrap analysis (Supplementary Material 20) indicates greater variability in centile estimates for younger (< 12 years) and older individuals (> 75 years), particularly for the 97.5% centile.

3.4. Comparison to previously published curves

The intracranial curves were compared to Satanin et al. (2024b) work for children. We found no statistical significance between the 3rd ($p = 0.49$,$p = 0.09$), 50th ($p = 0.14$,$p = 0.06$), and 97th ($p = 0.87$,$p = 0.38$) centile curves for both male and females individuals (Supplementary Figure 21 and 22).

The comparison of our lateral ventricle curves with those of Maragkos et al. (2021) (Fig. 6), resulted in statistically significant differences in the 2.5% and 97.5% quantiles of male curves, as well as in the median and 2.5% quantile of female curves (Fig. 6).

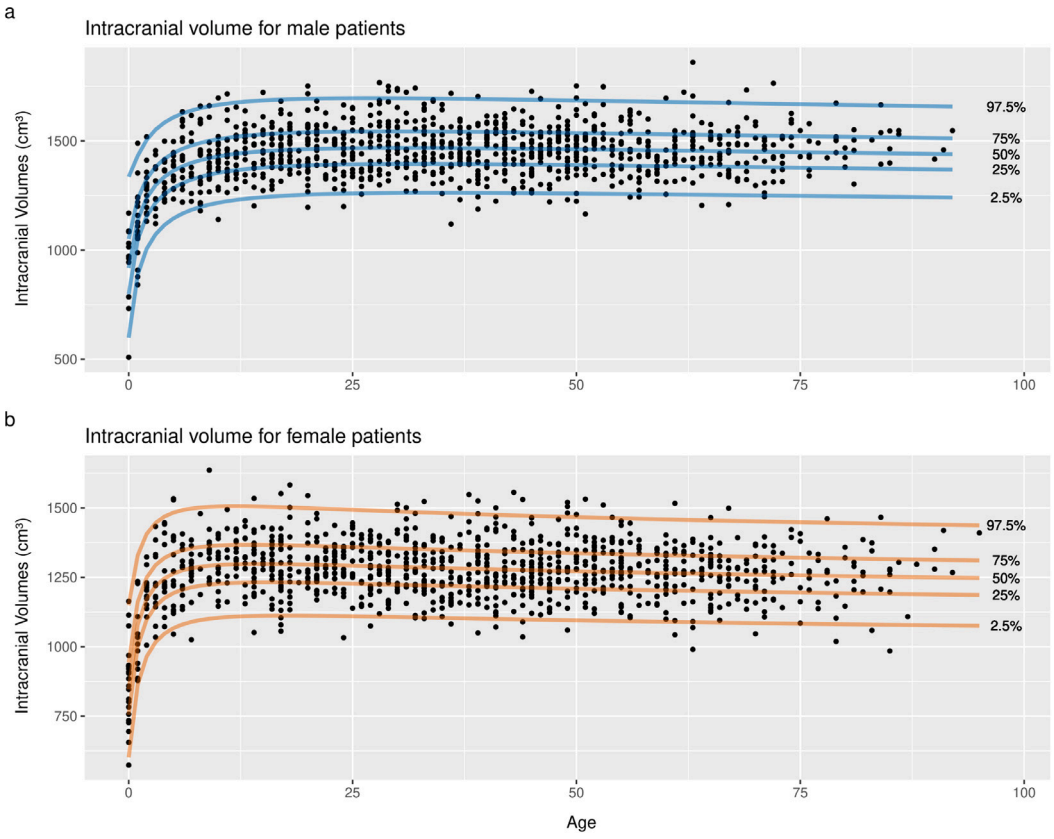

Fig. 2. Centile curves for the intracranial volumes (cm^3) for male and female individuals. Black dots represent the exams used to fit the curves.

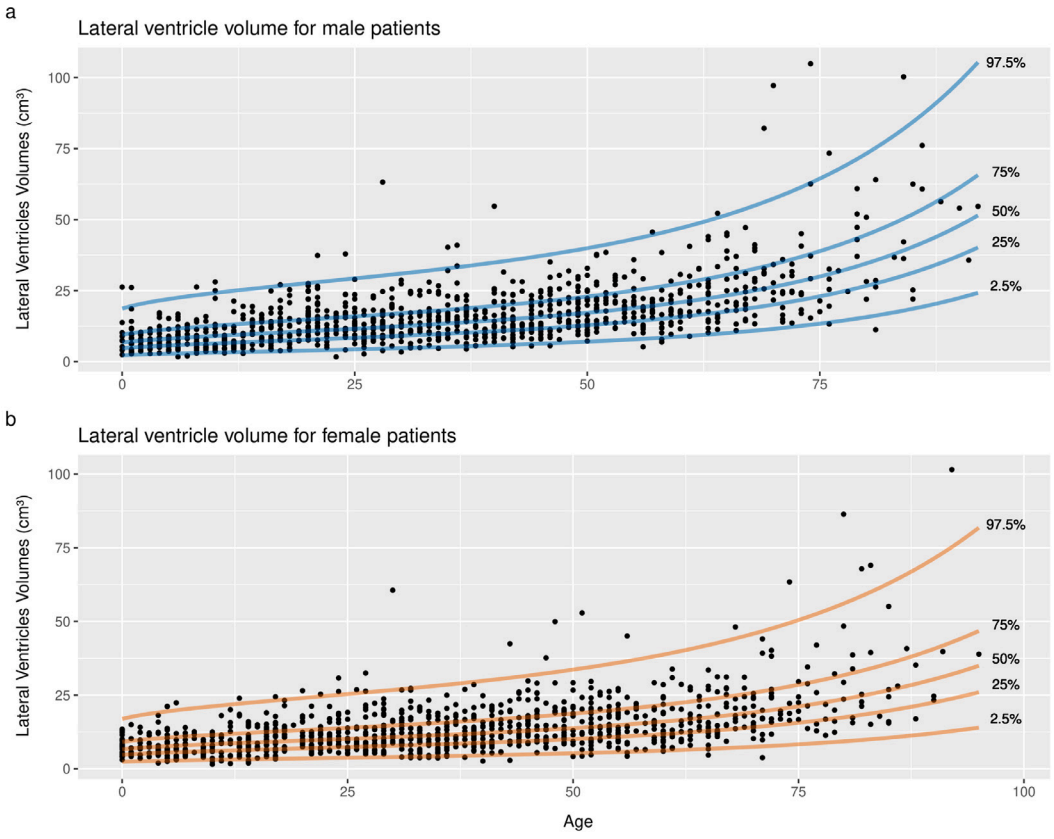

Fig. 3. Centile curves for the ventricular volumes (cm^3) for male and female individuals. Black dots represent the exams used to fit the curves.

Table 2
Median and interquartile range ($Q_{25\%} - Q_{75\%}$) of ICV, LVV, and age.

Variable	Male	Female	Kruskal–Wallis	η^2	Anderson–Darling
Intracranial volume sample (cm^3)	1,442.73 (1364.32-1521.76)	1,272.73 (1207.59-1340.28)	<0.001	0.36	<0.001
Age in the intracranial volumes sample	34 (17-50)	36 (18-54)	0.05	–	<0.001
Lateral ventricular volume sample (cm^3)	13.98 (9.40-20.71)	11.89 (8.17-17.53)	<0.001	0.01	<0.001
Age in the lateral ventricular sample	34 (17-51)	36 (18-54)	0.08	–	<0.001

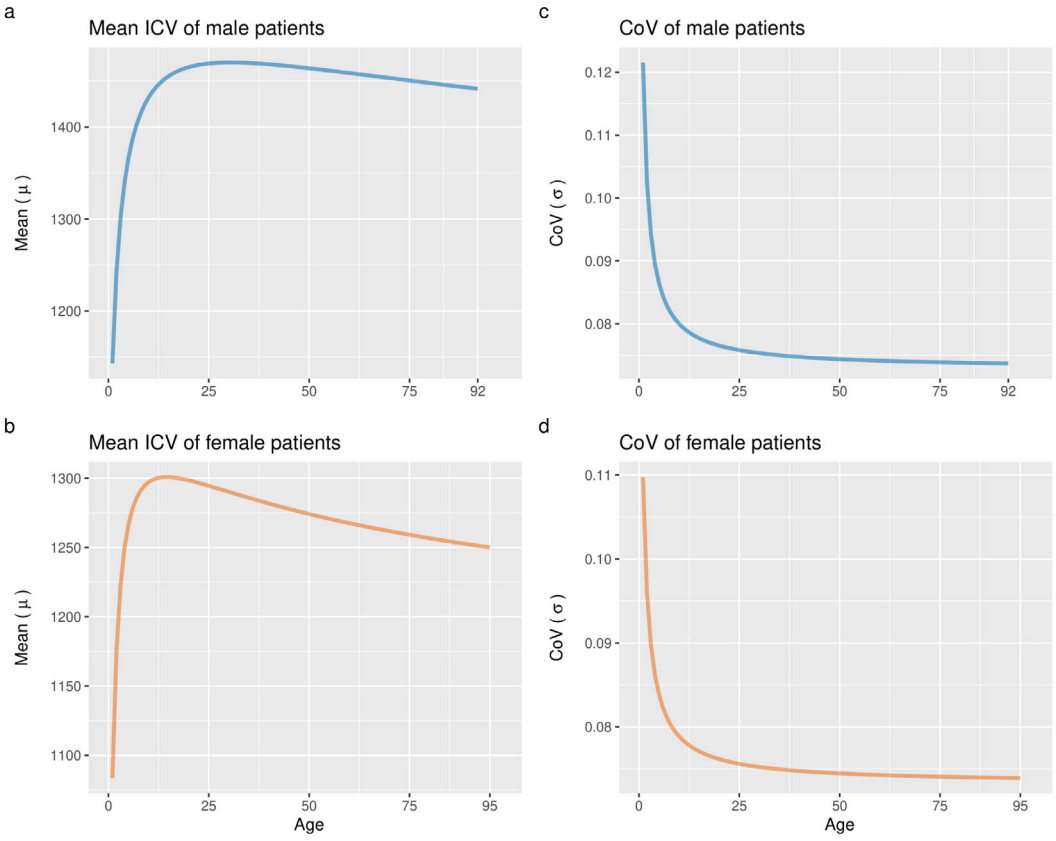

Fig. 4. Mean and Coefficient of Variation (CoV) for intracranial volume (ICV) models. Panels (a) and (b) show the mean ICV, and (c) and (d) show the CoV for males and females, respectively.

3.5. Preliminary validation

To illustrate the clinical application of these normative curves, we analyzed six pathological cases, including congenital anomalies and acquired conditions. When plotted on our curves, these cases consistently appeared as outliers, highlighting their deviation from normative values (Supplementary Table 2 and Supplementary Images 25 to 28).

4. Discussion

This study aimed to establish normative curves for ICV and LVV, potentially providing radiologists and clinicians with valuable tools to detect and monitor abnormal changes in brain volume in individuals with neurological disorders. As automated tools for segmenting and quantifying brain regions become more prevalent (Moraes et al., 2023; Maragkos et al., 2021; Kellogg et al., 2023), these curves serve as essential references for distinguishing normal from pathological cases. The creation of normative curves addresses the global need for more accurate assessments, diagnoses, and treatment plans, especially considering the literature's lack of CT-derived normative values for brain regions. CT offers several advantages, including being less resource-intensive, faster, and more widely available.

We employed a rigorous methodology to conduct the proposed analyses. Without established sample size guidelines for normative brain structure curves, its size was determined based on prior literature concerning pediatric neuropsychological norms (Bridges and Holler, 2007). Most existing data rely on convenience samples or public databases (Nasser et al., 2024; Cutler et al., 2020; Peterson et al., 2021). Careful sample planning provides numerous benefits. First, tailoring the curves to a specific population reduces the risk of over- or underestimating volumes, which can occur when using data from other populations (Bethlehem et al., 2022). Second, convenience samples often fail to fully represent the target population, leading to potential bias, particularly in underrepresented age groups. In the short term, our sample planning results in a more manageable number of images. In the long term, it establishes a foundation for refining the model and improving curve accuracy across specific age groups.

Using GAMLSS for flexible modeling allowed us to capture nonlinear trends between age and brain volumes while also enabling the interpretation of this relationship. Models were fitted separately by sex, as the data revealed statistically significant sexual dimorphism. Females exhibited smaller median ICV and LVV than males, consistent with previous findings (Eliot et al., 2021; Ruigrok et al., 2014). Nonparametric methods, such as penalized cubic B-splines, are commonly used in normative studies of intracranial and ventricular volumes based on MRI data (Nasser et al., 2024). However, with smaller sample sizes spanning wide age ranges, this approach can lead to overfitting and introduce artificial fluctuations in growth trajectories. In contrast, the fractional

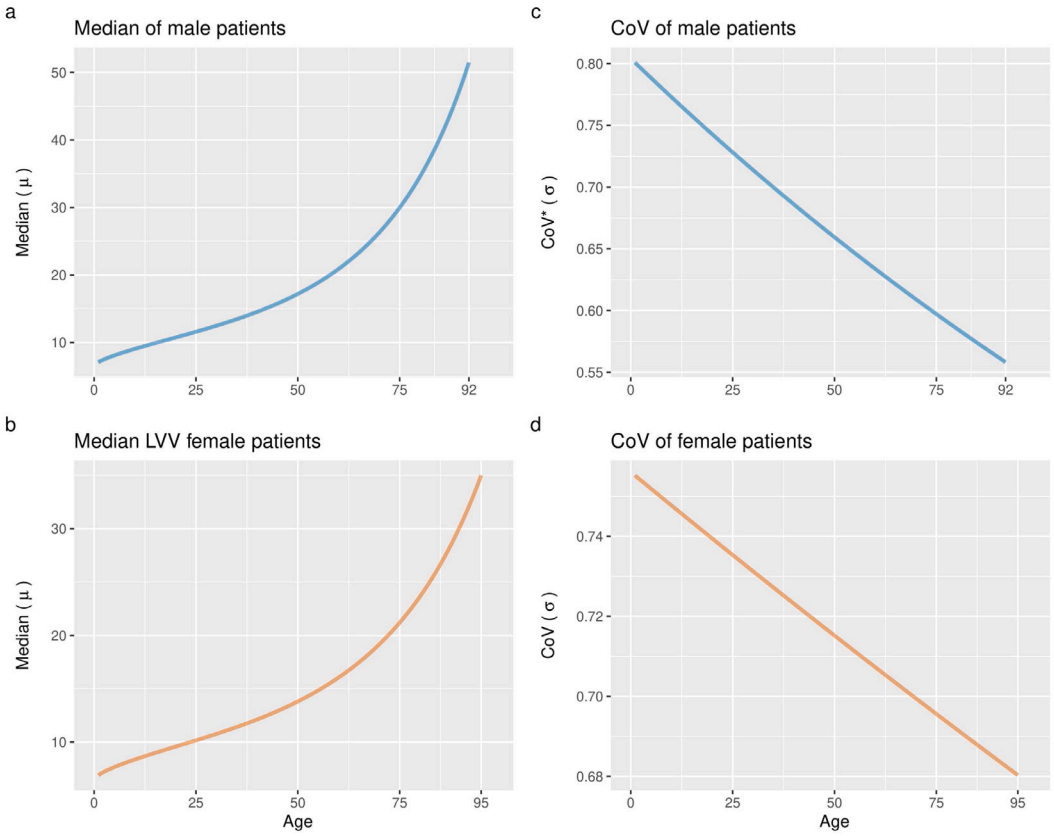

Fig. 5. Median and Coefficient of Variation (CoV) for lateral ventricular volume (LVV) models. Panels (a) and (b) show the median LVV, and (c) and (d) show the CoV for males and females, respectively. τ and ν remain fixed throughout the lifespan.

polynomials used in this study offered a more precise fit and produced clinically interpretable curves.

Luo et al. (2015) conducted a chi-square analysis to assess their models and also observed high p-values for their studied structures. This demonstrates our model's good performance in reproducing the data quantiles. Residual analysis revealed a potential overestimation of mean ICV in males aged 29–34 years. For the LVV curves, signs of misfit were detected in the median for males aged 8–21 years, the CoV for those aged 48–55 years, and the kurtosis for ages 22–28 years. In the female curves, median misfits were observed in individuals aged 44–50 and 58–67 years, along with misfits in kurtosis for those aged 22–28 years. The randomized quantile residual plots did not present strong indications of overall misfit for all models. Although such deviations are expected even with a well-fitted model, they highlight areas where the current fits could be improved. Normative studies often rely on R^2 (Potvin et al., 2016; Kalucki et al., 2020) or Q–Q plots (Cutler et al., 2020) to assess model quality. However, R^2 tends to favor models with more covariates without fully capturing the goodness of fit, while Q–Q plots provide only a broad overview, lacking detail on age-specific misfits. Neglecting residual analysis risks selecting suboptimal models by overlooking significant trends and over- or underestimations in specific age groups. This should be especially harmful to the sensitivity of detecting abnormal cases, as changes in the location and shape of the chosen probability distribution will affect the 2.5% and 97.5% percentile curves.

Regarding the interpretation of our models, early-life variability in ICV likely reflects underlying neurodevelopmental processes, followed by stabilization as growth plateaus in adulthood. Females tend to exhibit an earlier and more pronounced decline in ICV compared to males. Two hypotheses may account for this pattern. First, frontal hyperostosis – a benign, idiopathic overgrowth of the inner frontal bones, often extending to parietal regions – may contribute to reduced measurable ICV. This condition is commonly incidental, with a reported post-mortem prevalence of 12%, and 87% of severe cases observed in women over 65 years of age (Raikos et al., 2011). Second, generalized age-related skull thickening, which may differ by sex, could also reduce the intracranial cavity and bias ICV estimates (Royle et al., 2013). These structural changes may represent compensatory cranial remodeling processes aimed at preserving intracranial pressure homeostasis in response to age-related reductions in parenchymal volume (Urban et al., 2016). Although we did not assess cranial bone volume in this study, future research incorporating direct measures of bone thickness or cranial vault volume could help disentangle these effects. The median LVV, on the other hand, increases exponentially throughout life. These findings are consistent with those reported by Bethlehem et al. (2022), who describe an exponential trajectory for both the median volume and rate of change of the ventricular system (including the third and fourth ventricles). The coefficient of variation (CoV) for ICV and LVV decreases, reflecting a shift from high variability between individuals in early life to greater stability in adulthood. This trend likely results from neurodevelopmental consolidation and a more predictable trajectory of age-related changes. As these conclusions are derived from visual inspection, further statistical analysis is required for validation.

Few studies have established sex- and age-specific CT-derived normative data for brain structures. Kellogg et al. (2023) analyzed ventricular volumes from 866 CT scans, providing reference ranges for males and females aged 18–99 but excluding individuals under 18. Maragkos et al. (2021) generated normative values from 6,239 scans of individuals aged 3–90 years. However, both studies lacked statistical sample size calculations for each age group and relied solely on descriptive statistics for binned age ranges. This limited the interpretation of the relationship between volume and age across the lifespan and hindered uncertainty analysis, such as using bootstrap to generate confidence intervals for their centile estimates. In contrast, Satanin et al. (2024b)

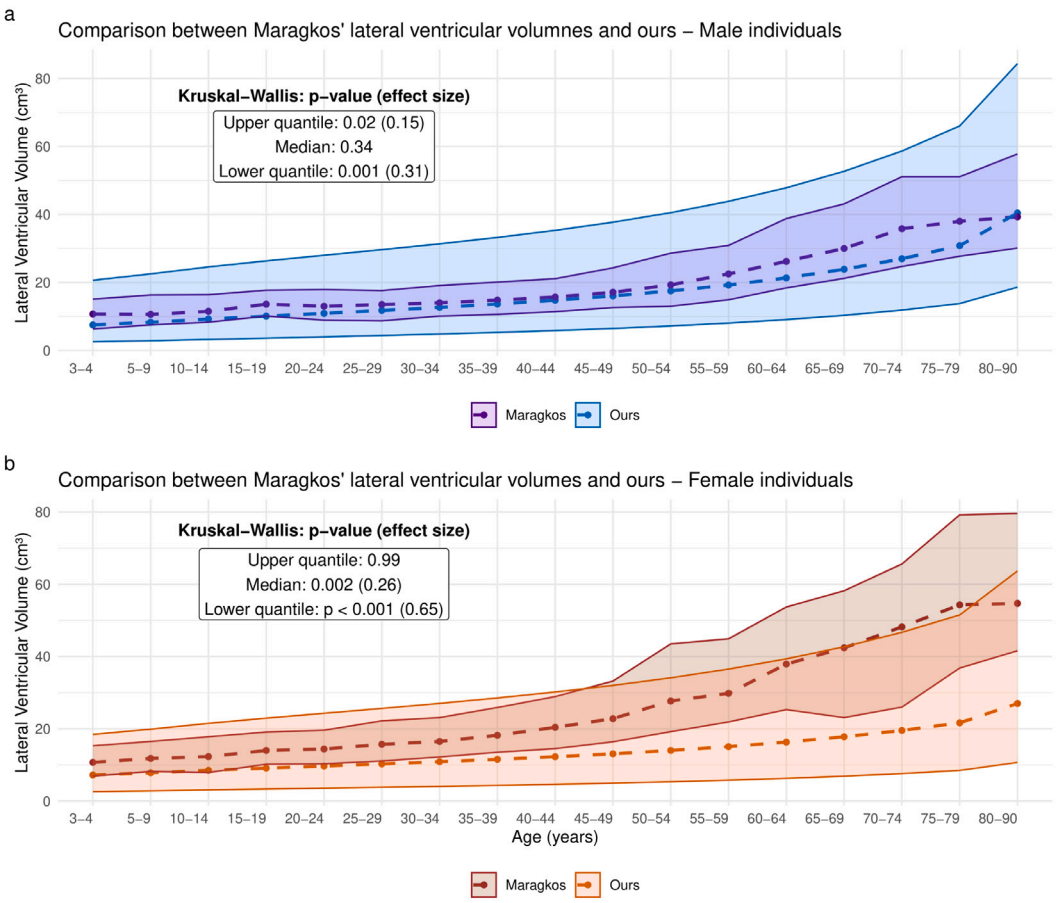

Fig. 6. Comparisons between our lateral ventricular curves and Maragkos'. (a) Comparison for male individuals. (b) Comparison for female individuals.

focused on a sample of 673 CT exams for children (aged 0–17 years) to construct normative curves for ICV using a similar approach to ours with GAMLSS and the Lambda-Mu-Sigma (LMS) method. This study underscores the importance of developing sex- and age-specific reference curves in pediatric neurology, in which precise volume measurements are essential for the early detection of brain abnormalities. When we compared our curves with these studies, no significant statistical difference was found between our ICV curve and Satanin's. In contrast, Maragkos's LVV curves differed from ours in the median and 2.5th centile for females, as well as in the 2.5th and 97.5th centiles for males. This discrepancy may be attributed to over- or underrepresented age groups.

Dima et al. (2021) have established MRI-based normative values for total intracranial volume and constructed distinct growth curves for the left and right lateral ventricles. Notably, the trajectories observed in their curves align closely with those identified in our study. Similarly, Bethlehem et al. (2022) have developed normative charts for total brain volume and total ventricular cerebrospinal fluid. While these regions are not identical to those assessed in our analysis, they are anatomically related—the brain (encephalon) constitutes a major subregion of the intracranial volume, and the lateral ventricles represent the largest component of the ventricular system. Their overall observed trends are also consistent with our findings. To further evaluate the similarities between CT and MRI, future studies should focus on comparing the normative ranges of the same anatomical structures across both modalities. Such efforts could also help establish modality-independent normative standards, particularly if anatomical definitions are harmonized across studies.

The bootstrap analysis provided 95% confidence intervals for all centile estimates, allowing us to assess the stability and reliability of the models. For both ICV and LVV curves, the confidence intervals were wider in the early years and older age groups. The broader early-year intervals likely reflect the higher variability observed in the formative stages. Since the models employed age as integers rather than continuous values, finer distinctions – such as between a two-month-old and an eleven-month-old – were not captured. Conversely, in older age groups, this variability may be attributed to smaller sample sizes. While these edge effects can be mitigated by oversampling infants and elderly individuals during sample size planning (Cole, 2021), acquiring normative CT scans for children is challenging due to the risks associated with radiation exposure, making CT less commonly performed in this age group.

Our qualitative analysis of the outlier cases revealed that most scans showed age-appropriate brain parenchyma. This suggests that the 1.5*IQR threshold for defining outliers may be overly sensitive and fail to capture normal biological variability. A few scans exhibited suboptimal segmentation, consistent with previous findings of substantial but imperfect agreement among neuroradiologists (Pinto et al., 2024). Only three scans revealed unexpected brain findings for age. This highlights a limitation of our study, as it was not feasible to comprehensively review all scans, potentially leading to mislabeling some abnormal scans as normal.

In clinical practice, the assessment of ICV and LVV on CT and MRI often relies on subjective visual inspection or two-dimensional indices, with three-dimensional measurements rarely applied. This subjective approach, combined with limited analysis, introduces variability and potential inaccuracies, especially when comparing patients to normative standards. The development of CT-derived normative curves for ICV and LVV provides a more objective and standardized method for evaluating brain volumes, offering significant clinical benefits.

First, these curves provide radiologists and clinicians with a reliable reference for detecting subtle deviations from normal brain volumes—variations that may go unnoticed with subjective assessments. This is particularly useful for evaluating conditions such as hydrocephalus or other volumetric changes, in which early detection is crucial for timely intervention. Second, integrating these normative curves into automated segmentation tools enhances diagnostic accuracy by offering real-time, data-driven comparisons to age- and sex-specific norms. This shift toward objective, quantitative assessments reduces variability between radiologists and institutions, leading to more consistent and reliable diagnoses. An automated flagging system within radiologists' worklists could also streamline workflow efficiency by prioritizing flagged cases, potentially reducing reporting times and expediting patient management. While our preliminary clinical validation is primarily illustrative, it demonstrates the potential of these normative curves in triaging abnormal findings and improving radiology workflows. Finally, as medicine increasingly embraces quantitative tools, clinicians must adapt to interpreting volumetric data and understanding its relevance to actual pathological changes. While this transition involves a learning curve, it fosters a more precise, data-driven approach to neuroimaging. Using CT-derived normative curves increases the potential for early detection and improved patient outcomes, particularly in settings where MRI is less accessible or where CT is preferred for its speed and availability (Cauley et al., 2021; Rosenkrantz et al., 2015). Future studies should validate these curves in larger, more diverse cohorts and assess their impact on diagnostic accuracy, workflow efficiency, and clinical decision-making. Multi-center trials could further evaluate automated flagging systems across imaging protocols, while comparisons with MRI-based volumetric analysis could also strengthen the clinical utility of CT-derived curves.

This study has additional limitations. Its single-center, cross-sectional design may limit the generalizability of the findings. The normality criteria were based solely on radiological assessments of the brain parenchyma (excluding the cranial vault and subarachnoid space) without incorporating clinical evaluations. Evaluating normality in CT scans is inherently subjective, particularly when determining whether radiological findings align with expectations for a specific age. While this morphological approach lacks clinical context, it remains valuable for imaging workflows that frequently rely on such criteria. This limitation is mitigated by the study's primary focus on imaging data. Future research should prioritize longitudinal studies to better capture intracranial volume dynamics over time and integrate clinical data for a more comprehensive understanding of neurological development and health. Further studies could also explore the impact of varying scan acquisition parameters to evaluate how they influence the performance of normative curves.

5. Conclusion

This study provides comprehensive normative curves for ICV and LVV based on CT scans, offering sex- and age-specific data to enhance diagnostic accuracy in conditions where precise volume measurements are critical for patient management. Notably, we employed sample size calculations that considered specific demographic factors and modeling techniques to capture non-linear trends between age and brain volumes, improving the precision of the normative curves. These CT-based curves have the potential to enhance diagnostic consistency, especially in environments with restricted access to MRI facilities.

CRediT authorship contribution statement

Pedro Vinicius Alves Silva: Writing – original draft, Validation, Software, Methodology, Investigation, Formal analysis, Data curation. **Bruna Garbes Goncalves Pinto:** Writing – original draft, Investigation, Data curation, Conceptualization. **Gabriel Ferracioli:** Writing – review & editing, Writing – original draft, Data curation. **Klaus Schumacher:** Writing – original draft, Methodology, Investigation, Data curation. **Artur Jose Marques Paulo:** Writing – review & editing, Writing – original draft, Data curation. **Luis Alvaro Correia:** Writing – review & editing, Validation, Methodology. **Mariana Curi:** Writing – review & editing, Validation, Methodology. **Mateus Trinconi Cunha:** Writing – review & editing, Writing – original draft. **Joselisa Peres Queiroz de Paiva:** Writing – review & editing, Project administration, Conceptualization. **Tatiana Larissa Medeiros Arcanjo Marques:** Writing – review & editing, Resources, Data curation. **Rafael Maffei Loureiro:** Writing – review & editing, Writing – original draft, Supervision, Resources, Project administration, Data curation.

Declaration of Generative AI and AI-assisted technologies in the writing process

The authors used ChatGPT-4o (OpenAI) to enhance the readability and language of this manuscript. Following its use, the authors thoroughly reviewed and edited the content, taking full responsibility for the final published version.

Declaration of competing interest

The authors declare the following financial interests/personal relationships which may be considered as potential competing interests: Pedro Vinicius Alves Silva reports a relationship with Ministry of Health of Brazil that includes: funding grants. Bruna Garbes Goncalves Pinto reports a relationship with Ministry of Health of Brazil that includes: funding grants. Gabriel Ferracioli reports a relationship with Ministry of Health of Brazil that includes: funding grants. Klaus Schumacher reports a relationship with Ministry of Health of Brazil that includes: funding grants. Artur Jose Marques Paulo reports a relationship with Ministry of Health of Brazil that includes: funding grants. Luis Alvaro Correia reports a relationship with Ministry of Health of Brazil that includes: funding grants. Joselisa Peres Queiroz de Paiva reports a relationship with Ministry of Health of Brazil that includes: funding grants. Tatiana Larissa Medeiros Arcanjo Marques reports a relationship with Ministry of Health of Brazil that includes: funding grants. Rafael Maffei Loureiro reports a relationship with Ministry of Health of Brazil that includes: funding grants. If there are other authors, they declare that they have no known competing financial interests or personal relationships that could have appeared to influence the work reported in this paper.

Acknowledgments

We would like to express our sincere gratitude to Paula Bresciani Martins de Andrade for her valuable contribution in revising the final version of the manuscript. Her insightful feedback and suggestions significantly improved the quality and clarity of this work. We also greatly appreciate the time and effort of all of our team member and collaborators.

This project was funded by the Program for Support to the Institutional Development of the Unified Health System (PROADI-SUS, 01/2023; NUP: 25000.156740/2023-25) in collaboration with Hospital Israelita Albert Einstein.

Appendix A. Supplementary data

Supplementary material related to this article can be found online at https://doi.org/10.1016/j.neuroimage.2025.121272.

Data availability

Data will be made available on request.

References

Bethlehem, R.A., Seidlitz, J., White, S.R., Vogel, J.W., Anderson, K.M., Adamson, C., Adler, S., Alexopoulos, G.S., Anagnostou, E., Areces-Gonzalez, A., et al., 2022. Brain charts for the human lifespan. Nature 604 (7906), 525–533. http://dx.doi.org/10.1038/s41586-022-04554-y.

Billot, B., Greve, D.N., Puonti, O., Thielscher, A., Leemput, K.V., Fischl, B., Dalca, A.V., Iglesias, J.E., ADNI, 2023. SynthSeg: Segmentation of brain MRI scans of any contrast and resolution without retraining. Med. Image Anal. 86, 102789. http://dx.doi.org/10.1016/j.media.2023.102789.

Borghi, E., de Onis, M., Garza, C., den Broeck, J.V., Frongillo, E.A., Grummer-Strawn, L., Buuren, S.V., Pan, H., Molinari, L., Martorell, R., Onyango, A.W., Martines, J.C., 2005. Construction of the world health organization child growth standards: Selection of methods for attained growth curves. Stat. Med. 25 (2), 245–265. http://dx.doi.org/10.1002/sim.2227.

Breakey, W., Knoops, P.G., Borghi, A., 2017. Intracranial volume measurement: A systematic review and comparison of different techniques. J. Craniofacil Surg. 28, 1746–1751. http://dx.doi.org/10.1097/SCS.0000000000003929.

Bridges, A.J., Holler, K.A., 2007. How many is enough? Determining optimal sample sizes for normative studies in pediatric neuropsychology. Child Neuropsychol. 13, 528–538. http://dx.doi.org/10.1080/09297040701233875.

Cauley, K., Hu, Y., Fielden, S., 2021. Head CT: toward making full use of the information the X-rays give. Am. J. Neuroradiol. 42 (8), 1362–1369.

Cohen, J., 1988. Statistical Power Analysis for the Behavioral Sciences, second ed. Lawrence Erlbaum Associates, New York, http://dx.doi.org/10.4324/9780203771587.

Cole, T., 2021. Sample size and sample composition for constructing growth reference centiles. Stat. Methods Med. Res. 30 (2), 488–507. http://dx.doi.org/10.1177/0962280220958438.

Cutler, N.S., Srinivasan, S., Aaron, B.L., Anand, S.K., Kang, M.S., Altshuler, D.B., Schermerhorn, T.C., Hollon, T.C., Maher, C.O., Khalsa, S.S.S., 2020. Normal cerebral ventricular volume growth in childhood. J. Neurosurg.: Pediatr. 26 (5), 517–524. http://dx.doi.org/10.3171/2020.5.PEDS20178.

Dima, D., Modabbernia, A., Papachristou, E., Doucet, G.E., Agartz, I., Aghajani, M., Akudjedu, T.N., Albaiges-Ezagirre, A., Alnaes, D., Alpert, K.I., Andersson, M., Andreassen, O.A., Asherson, P., Banaschewski, T., Bargallo, N., Baumeister, S., Baur-Streubel, R., Bertolino, A., Bonvino, A., Boomsma, D.I., Bora, E., Bourque, J., Brandies, D., Breier, A., Brodaty, H., Brouwer, R.M., Buitelaar, J.K., Busatto, G.F., Buckner, R.L., Calhoun, V., Canales-Rodríguez, E.J., Cannon, D.M., Caseras, X., Castellanos, F.X., Cervenka, S., Chaim-Avancini, T.M., Ching, C.R.K., Chubar, V., Clark, V.P., Conrod, P., Conzelmann, A., Crespo-Facorro, B., Crivello, F., Crone, E.A., Dannlowski, U., Dale, A.M., Desrivieres, S., De Geus, E.J., de Haan, L., de Zubicaray, G.I., den Braber, A., Dickie, E.W., Di Giorgio, A., Doan, N.T., Dørum, E.S., Ehrlich, S., Erk, S., Espeseth, T., Fatouros-Bergman, H., Fisher, S.E., Fouche, J.P., Franke, B., Frodl, T., Fuentes-Claramonte, P., Glahn, D.C., Gotlib, I.H., Grabe, H.J., Grimm, O., Groenewold, N.A., Grotegerd, D., Gruber, O., Gruner, P., Gur, R.E., Gur, R.C., Hahn, T., Harrison, B.J., Hartman, C.A., 2021. Subcortical volumes across the lifespan: Data from 18,605 healthy individuals aged 3–90 years. Hum. Brain Mapp. 42 (13), 4735–4755. http://dx.doi.org/10.1002/hbm.25320.

Dunn, P.K., Smyth, G.K., 1996. Randomized quantile residuals. J. Comput. Graph. Statist. 5 (3), 236–244. http://dx.doi.org/10.2307/1390802.

Eliot, L., Ahmed, A., Khan, H., Patel, J., 2021. Dump the "dimorphism": Comprehensive synthesis of human brain studies reveals few male-female differences beyond size. Neurosci. Biobehav. Rev. 125, 667–697.

Fang, C., Ji, M., Dong, C., Li, J., Ye, X., 2022. Comparing the increased intracranial volume from different surgical methods for syndromic craniosynostosis. J. Craniofac. Surg. 33 (8), 2529–2533. http://dx.doi.org/10.1097/SCS.0000000000008791.

Geethanath, S., Vaughan, Jr., J.T., 2019. Accessible magnetic resonance imaging: A review. J. Magn. Reson. Imaging http://dx.doi.org/10.1002/jmri.26638.

González-Villà, S., Oliver, A., Valverde, S., Wang, L., Reyer Zwiggelaar, X.L., 2016. A review on brain structures segmentation in magnetic resonance imaging. Artif. Intell. Med. 73, 45–69. http://dx.doi.org/10.1016/j.artmed.2016.09.001.

Hedderich, D.M., Dieckmeyer, M., Andrisan, T., Ortner, M., Grundl, L., Schön, S., Suppa, P., Finck, T., Kreiser, K., Zimmer, C., et al., 2020. Normative brain volume reports may improve differential diagnosis of dementing neurodegenerative diseases in clinical practice. Eur. Radiol. 30, 2821–2829.

Huff, T.J., Ludwig, P.E., Salazar, D., Cramer, J.A., 2019. Fully automated intracranial ventricle segmentation on CT with 2D regional convolutional neural network to estimate ventricular volume. Int. J. Comput. Assist. Radiol. Surg. 14, 1923–1932. http://dx.doi.org/10.1007/s11548-019-02038-5.

Huisman, S., Maspero, M., Philippens, M., Verhoeff, J., David, S., 2024. Validation of SynthSeg segmentation performance on CT using paired MRI from radiotherapy patients. NeuroImage 303, 120922. http://dx.doi.org/10.1016/j.neuroimage.2024.120922.

Huo, Y., Asman, A.J., Plassard, A.J., Landman, B.A., 2017. Simultaneous total intracranial volume and posterior fossa volume estimation using multi-atlas label fusion. Hum. Brain Mapp. 38 (2), 599–616. http://dx.doi.org/10.1002/hbm.23432.

IBGE, 2024. IBGE populations projections. https://www.ibge.gov.br/estatisticas/sociais/populacao/9109-projecao-da-populacao.html?=&t=resultados. (Accessed 19 May 2024).

Kalucki, S.A., Lardi, C., Garessus, J., Kfoury, A., Grabherr, S., Burnier, M., Pruijm, M., 2020. Reference values and sex differences in absolute and relative kidney size. A Swiss autopsy study. BMC Nephrol. 21, 289. http://dx.doi.org/10.1186/s12882-020-01946-y.

Kellogg, R.T., Park, M.S., Snyder, M.H., Marino, A., Patel, S., Feng, X., Vargas, J., 2023. Establishment of age-and sex-specific reference cerebral ventricle volumes. World Neurosurg. 175, e976–e983.

Klasson, N., Olsson, E., Rudemo, M., Eckerström, C., Malmgren, H., Wallin, A., 2015. Valid and efficient manual estimates of intracranial volume from magnetic resonance images. BMC Med. Imaging 15 (5), http://dx.doi.org/10.1186/s12880-015-0045-4.

Kuller, L.H., Lopez, O.L., Jagust, W.J., Becker, J.T., DeKosky, S.T., Lyketsos, C., Kawas, C., Breitner, J.C.S., Fitzpatrick, A., Dulberg, C., 2005. Determinants of vascular dementia in the cardiovascular health cognition study. Neurology 64 (9), 1548–1552. http://dx.doi.org/10.1212/01.WNL.0000160115.55756.DE.

van Loenhoud, A.C., Groot, C., Vogel, J.W., van der Flier, W.M., Ossenkoppele, R., 2018. Is intracranial volume a suitable proxy for brain reserve? Alzheimer's Res. Ther. 10 (1), 91. http://dx.doi.org/10.1186/s13195-018-0408-5.

Luo, W., Airriess, C., Albright, J., 2015. The NeuroQuant Normative Database Comparing Individual Brain Structures. Technical Report, Cortechs Labs, URL: https://www.cortechs.ai/wp-content/uploads/2018/10/Normative-Database-White-Paper.pdf. (Last access: 8 March 2025).

Malone, I.B., Leung, K.K., Clegg, S., Barnes, J., Whitwell, J.L., Ashburner, J., Fox, N.C., Ridgway, G.R., 2015. Accurate automatic estimation of total intracranial volume: a nuisance variable with less nuisance. Neuroimage 104, 366–372. http://dx.doi.org/10.1016/j.neuroimage.2014.09.034.

Maragkos, G.A., Filippidis, A.S., Chilamkurthy, S., Salem, M.M., Tanamala, S., Gomez-Paz, S., Rao, P., Moore, J.M., Papavassiliou, E., Hackney, D., et al., 2021. Automated lateral ventricular and cranial vault volume measurements in 13,851 patients using deep learning algorithms. World Neurosurg. 148, e363–e373.

Moraes, L., Lago, L., Moura, L., Acamine, P., Estevam, P., Kallas, L., Loureiro, R., Paiva, J., Szarf, G., Amaro, Jr., E., et al., 2023. Multi-task deep learning model for the automated segmentation of neuroimages in real-world ct scans. http://dx.doi.org/10.2139/ssrn.4630905, Available at SSRN 4630905.

Mosley, Jr., T.H., Knopman, D.S., Catellier, D.J., Bryan, N., Hutchinson, R.G., Grothues, C.A., Folsom, A.R., Cooper, L.S., Burke, G.L., Liao, D., Szklo, M., 2005. Cerebral MRI findings and cognitive functioning: the atherosclerosis risk in communities study. Neurology 64 (12), 2056–2062. http://dx.doi.org/10.1212/01.WNL.0000165985.97397.88.

Nasser, S.N., Venugopal, V.K., Veenstra, C., Johansson, P., 2024. Age-stratified assessment of brain volumetric segmentation on the Indian population using quantitative magnetic resonance imaging. Clin. Neuroradiol. 1–11. http://dx.doi.org/10.1007/s00062-023-01374-z.

Nestor, S.M., Rupsingh, R., Borrie, M., Smith, M., Accomazzi, V., Wells, J.L., Fogarty, J., Bartha, R., Alzheimer's Disease Neuroimaging Initiative, 2008. Ventricular enlargement as a possible measure of Alzheimer's disease progression validated using the Alzheimer's disease neuroimaging initiative database. J. Craniofac. Surg. 131(Pt 9), 2443–2454. http://dx.doi.org/10.1093/brain/awn146.

Pahwa, B., Bali, O., Goyal, S., Kedia, S., 2021. Applications of machine learning in pediatric hydrocephalus: a systematic review. Neurol. India 69 (Suppl 2), S380–S389.

Peterson, M.R., Cherukuri, V., Paulson, J.N., Ssentongo, P., Kulkarni, A.V., Warf, B.C., Monga, V., Schiff, S.J., 2021. Normal childhood brain growth and a universal sex and anthropomorphic relationship to cerebrospinal fluid. J. Neurosurg.: Pediatr. 28 (4), 458–468. http://dx.doi.org/10.3171/2021.2.PEDS201006.

Peterson, M., Warf, B.C., Schiff, S.J., 2018. Normative human brain volume growth. J. Neurosurg.: Pediatr. 21 (5), 478–485. http://dx.doi.org/10.3171/2017.10.PEDS17141.

Pinto, B.G.G., Olegário, T.M.M., Silva, P.V.A., Ferracioli, G.M., Paulo, A.J.M., 2024. Clinical validation of a deep learning model for segmenting and quantifying intracranial andventricular volumes on computed tomography. http://dx.doi.org/10.21203/rs.3.rs-4947326/v1, Preprint.

Potvin, O., Mouiha, A., Dieumegarde, L., Duchesne, S., 2016. Normative data for subcortical regional volumes over the lifetime of the adult human brain. NeuroImage 137, 9–20. http://dx.doi.org/10.1016/j.neuroimage.2016.05.016.

Quon, J.L., Han, M., Kim, L.H., Koran, M.E., Chen, L.C., Lee, E.H., Wright, J., 2021. Artificial intelligence for automatic cerebral ventricle segmentation and volume calculation: a clinical tool for the evaluation of pediatric hydrocephalus. J. Neurosurg. 27 (2), 131–138. http://dx.doi.org/10.3171/2020.6.PEDS20251.

Raikos, A., Paraskevas, G.K., Yusuf, F., Kordali, P., Meditskou, S., Al-Haj, A., Brand-Saberi, B., 2011. Etiopathogenesis of hyperostosis frontalis interna: a mystery still. Ann. Anat.-Anat. Anz. 193 (5), 453–458. http://dx.doi.org/10.1016/j.aanat.2011.05.004.

Ritvanen, A.G., de Oliveira, M.E., Koivikko, M.P., Hallila, H.O., Haaja, J.K., Koljonen, V.S., Leikola, J.P., Hukki, J.J., Paulasto-Kröckel, M.M., 2013. Mesh-based method for measuring intracranial volume in patients with craniosynostosis. Int. J. Comput. Assist. Radiol. Surg. 8 (5), 703–709. http://dx.doi.org/10.1007/s11548-013-0822-x.

Rosenkrantz, A.B., Mendiratta-Lala, M., Bartholmai, B.J., Ganeshan, D., Abramson, R.G., Burton, K.R., John-Paul, J.Y., Scalzetti, E.M., Yankeelov, T.E., Subramaniam, R.M., et al., 2015. Clinical utility of quantitative imaging. Academic Radiol. 22 (1), 33–49.

Royle, N., Hernández, M.V., Maniega, S.M., Arabisala, B., Bastin, M., Deary, I., Wardlaw, J., 2013. Influence of thickening of the inner skull table on intracranial volume measurement in older people. Magn. Reson. Imaging 31 (6), 918–922.

Royston, P., Altman, D.G., 1994. Regression using fractional polynomials of continuous covariates: parsimonious parametric modelling. J. R. Stat. Soc. Ser. C. Appl. Stat. 43 (3), 429–453. http://dx.doi.org/10.2307/2986270.

Royston, P., Wright, E., 2000. Goodness-of-fit statistics for age-specific reference intervals. Stat. Med. 19, 2943–2962. http://dx.doi.org/10.1002/1097-0258(20001115)19:21<2943::aid-sim559>3.0.co;2-5.

Ruigrok, A.N., Salimi-Khorshidi, G., Lai, M.C., 2014. A meta-analysis of sex differences in human brain structure. Neurosci. Biobehav. Rev. 39, 34–50.

Sargolzaei, S., Sargolzaei, A., Cabrerizo, M., Chen, G., Goryawala, M., Pinzon-Ardila, A., Gonzalez-Arias, S.M., Adjouadi, M., 2015. Estimating intracranial volume in brain research: An evaluation of methods. Neuroinformatics 13 (4), 427–441. http://dx.doi.org/10.1007/s12021-015-9266-5.

Satanin, L., Evteev, A., Rudnev, S., Satanina, T., Roginsky, V., 2024a. Normative reference data for intracranial volume in children: The results of CT volumetry. Child's Nerv. Syst. 40, 1873–1879. http://dx.doi.org/10.1007/s00381-024-06318-7.

Satanin, L., Evteev, A., Rudnev, S., Satanina, T., Roginsky, V., 2024b. Normative reference data for intracranial volume in children: The results of CT volumetry. Child's Nerv. Syst. 1–7.

Schipper, J.A.M., van Lieshout, M.J., Böhringer, S., Padwa, B.L., Robben, S.G., van Rijn, R.R., Koudstaal, M.J., Lequin, M.H., Wolvius, E.B., 2021. Modelling growth curves of the normal infant's mandible: 3D measurements using computed tomography. Clin. Oral Investig. 25, 6365–6375. http://dx.doi.org/10.1007/s00784-021-03937-1.

Stasinopoulos, M., Rigby, B., De Bastiani, F., 2022. Gamlss.foreach: Parallel computations for distributional regression. J. R. Stat. Soc. Ser. C. Appl. Stat. http://dx.doi.org/10.1111/j.1467-9876.2005.00510.x, URL: https://CRAN.R-project.org/package=gamlss.foreach.

Stasinopoulos, M.D., Rigby, R.A., Heller, G.Z., Voudouris, V., De Bastiani, F., 2017. Flexible Regression and Smoothing: Using GAMLSS in R. CRC Press, http://dx.doi.org/10.1201/b21973.

T.J. Cole, P.G., 1992. Smoothing reference centile curves: The LMS method and penalized likelihood. Stat. Med. 11, 1305–1319. http://dx.doi.org/10.1002/sim.4780111005.

Tohka, J., 2014. Partial volume effect modeling for segmentation and tissue classification of brain magnetic resonance images: A review. World J. Radiol. 6 (11), 855–864. http://dx.doi.org/10.4329/wjr.v6.i11.855.

Tomczak M., E., 2014. The need to report effect size estimates revisited. An overview of some recommended measures of effect size. TRENDS Sport. Sci. 1 (21), 19–25.

Urban, J.E., Weaver, A.A., Lillie, E.M., Maldjian, J.A., Whitlow, C.T., Stitzel, J.D., 2016. Evaluation of morphological changes in the adult skull with age and sex. J. Anat. 229 (6), 838–846.

Van Loenhoud, A.C., Groot, C., Vogel, J.W., Van Der Flier, W.M., Ossenkoppele, R., 2018. Is intracranial volume a suitable proxy for brain reserve? Alzheimer's Res. Ther. 10, 1–12.

Vita, A., Peri, L.D., Silenzi, C., Dieci, M., 2006. Brain morphology in first-episode schizophrenia: a meta-analysis of quantitative magnetic resonance imaging studies. Schizophr. Res. 82 (1), 75–88. http://dx.doi.org/10.1016/j.schres.2005.11.004.

Westman, E., Aguilar, C., Muehlboeck, J.-S., Simmons, A., 2013. Regional magnetic resonance imaging measures for multivariate analysis in Alzheimer's disease and mild cognitive impairment. Brain Topogr. 26 (1), 9–23. http://dx.doi.org/10.1007/s10548-012-0246-x.

Whitwell, J.L., Crum, W.R., Watt, H.C., Fox, N.C., 2001. Normalization of cerebral volumes by use of intracranial volume: implications for longitudinal quantitative MR imaging. Am. J. Neuroradiol. 22 (8), 1483–1489. http://dx.doi.org/10.1186/s12880-015-0045-4.

WHO, 2022. Global atlas of medical devices 2022. URL: https://www.who.int/publications/i/item/9789240062207. (Accessed 02 September 2024).